A microfluidic chemostat for experiments with bacterial and yeast cells

Alex Groisman[1], Caroline Lobo[2], HoJung Cho[2], J Kyle Campbell[1], Yann S Dufour[3], Ann M Stevens[3] & Andre Levchenko[2]

Bacteria and yeast frequently exist as populations capable of reaching extremely high cell densities. With conventional culturing techniques, however, cell proliferation and ultimate density are limited by depletion of nutrients and accumulation of metabolites in the medium. Here we describe design and operation of microfabricated elastomer chips, in which chemostatic conditions are maintained for bacterial and yeast colonies growing in an array of shallow microscopic chambers. Walls of the chambers are impassable for the cells, but allow diffusion of chemicals. Thus, the chemical contents of the chambers are maintained virtually identical to those of the nearby channels with continuous flowthrough of a dynamically defined medium. We demonstrate growth of cell cultures to densely packed ensembles that proceeds exponentially in a temperature-dependent fashion, and we use the devices to monitor colony growth from a single cell and to analyze the cell response to an exogenously added autoinducer.

Although commonly thought of as self-sufficient single-cell organisms, bacteria and yeast can establish communities of high morphological and functional complexity[1–8]. The density of growing bacterial and yeast colonies can reach extremely high values (for example, 10^{10}–10^{11} *Vibrio fischeri* cells/ml in the light organs of *Euprymna scolopes*[9]) that are hard to achieve in the laboratory using common *in vitro* techniques owing to the rapid depletion of nutrients and accumulation of metabolic waste. Batch culture chemostats are also inappropriate as the convective flow used to refresh the medium leads to extensive mixing and loss of cells, preventing formation of naturally occurring, morphologically complex multicellular superstructures. Flow chambers used to study biofilm formation or chemotaxis in adherent cells[10,11] are not suitable for cells without or with weak surface adhesion, including the common lab strains of bacterium *Escherichia coli* and yeast *Saccharomyces cerevisiae*. Therefore, at this point, there is a lack of devices that can be used to perform experiments with nonadherent cells growing to high densities in chemostatic conditions.

Custom-made microfluidic devices are being used increasingly in cell biology[12–14]. The bacterial applications include studies of chemotaxis[15], phenotypic heterogeneity[16] and 'social' interaction between motile *E. coli*[17]. Here we propose a microfluidic device made of a silicone elastomer polydimethylsiloxane (PDMS) that allows culture of cells in chemostatic and thermostatic conditions in an array of shallow microscopic chambers. The medium in the chambers can be quickly redefined to transiently expose the cells to an exogenous signal. The device was used to grow cell colonies to high density starting from as few as one cell, and monitor them for extended periods of time at a single-cell resolution.

RESULTS
Device design and operation
The microchemostat device (**Fig. 1**) was designed to confine growth of nonadherent cells inside small chambers of different sizes while keeping chemical contents of the medium inside the chambers consistently close to that of the medium fed from an outside reservoir. The main functional area of the chemostat is an array of parallel channels with continuous flowthrough of fresh medium and parallel rows of chambers between the channels (**Fig. 1a–c**). The channels and chambers have a depth, h_1, of ~ 6 μm. The channels are 150 μm wide; the chambers have a width, w, of ~ 100 μm and lengths of 70–200 μm (**Fig. 1** and **Supplementary Fig. 1** online). The channels and chambers are connected by capillaries, which are ~ 20 μm wide, ~ 40 μm apart from each other and have a depth, h_2, of ~ 0.6 μm and length, l, of ~ 25 μm. The low depth of the capillaries makes them impenetrable to *E. coli* cells (about 1 μm in diameter and 2–3 μm in length) and to other bacterial and yeast species (**Supplementary Fig. 2** online). The characteristic time of diffusive exchange between the chambers and the channels for small molecules with diffusion coefficient $D = 6 \times 10^{-6}$ cm^2/s, can be estimated as $wh_1l \div (Dh_2) \approx 40$ s, which is at least 50 times faster than the bacterial cell division cycle. The flow rate through the channels required to replace the medium adjacent to the chambers within 40 s is ~ 100 μm/s, and it should be sufficient for adequate refreshment of the chamber environment. The temperature on the chip is set and stabilized to within 0.5 °C by flow of water through a 0.3 mm–deep and 1.4 mm–wide channel that surrounds the array of channels

[1]Department of Physics, University of California San Diego, 9500 Gilman Dr., MC 0374, La Jolla, California 92093, USA. [2]Department of Biomedical Engineering and Whitaker Institute of Biomedical Engineering, Johns Hopkins University, Baltimore, Maryland 21218, USA. [3]Department of Biology, Virginia Polytechnic Institute and State University, Blacksburg, Virginia 24061, USA. Correspondence should be addressed to A.G. (agroisman@ucsd.edu) or A.L. (alev@bme.jhu.edu).
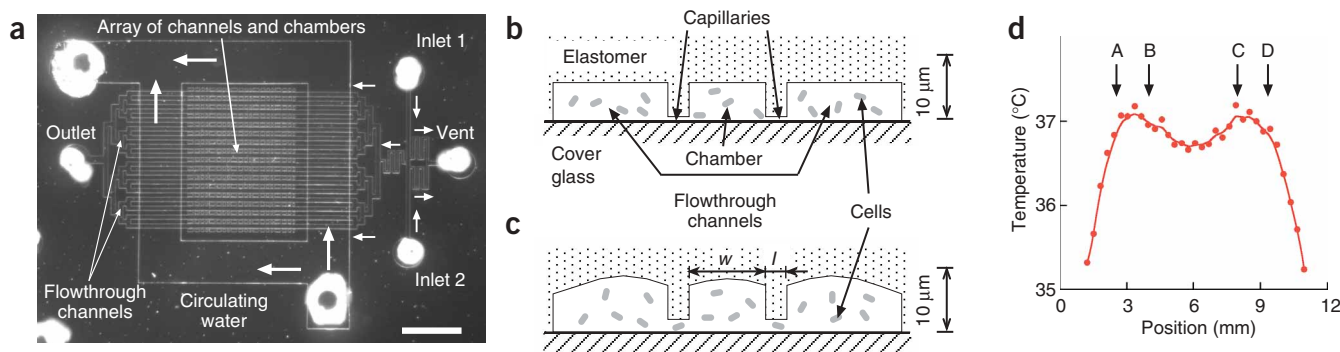
Figure 1 | Design and operation of the two-layer microfluidic device. (**a**) Micrograph of the PDMS device. Bar, 2 mm. Horizontal and vertical arrows show direction of flow. The chip has an array of 16 flowthrough channels and 340 chambers. Inlets 1 and 2 are symmetric and are connected to the array by a T junction. Each inlet is connected to the vent a short distance upstream of the T junction. The pressures applied to the inlets are adjusted so that medium from only one of the inlets is fed to the chamber array at any time, but there is always some flow from both inlets to the vent. Therefore, the streams from both inlets are always close to the T-junction, and the medium in the array is quickly replaced once the driving pressures are switched. (**b,c**) Schematic drawing of a cross-section of the array showing two channels, a chamber of width w and two capillaries of length l connecting the channels and the chamber. At low gauge pressure inside the device (**b**) the capillaries are impermeable to the cells, but they become permeable at high gauge pressure (**c**). (**d**) Temperature profile along a line going through the center of the device (a horizontal line at half-height in **a**) measured with an infrared camera. A and D, and B and C mark the outer and inner boundaries of the water circulation channel, respectively. Thermostatic water circulator was set at 37.0 °C. The room temperature was ~22 °C.

and chambers and is a part of the monolith PDMS device[18] (**Fig. 1a**, **Supplementary Fig. 1** and **Supplementary Methods** online).

The device is designed to prevent any active flow through the chambers and possible perturbation of cell position, motion or intercellular interaction that may result. On both the inlet and outlet sides (**Fig. 1a**), the branching from a single channel into the array of 16 parallel channels is binary and symmetric. This arrangement leads to equal flow rates through the channels, highly balanced pressures at capillaries on opposite sides of the chambers and thus very small flow through the chambers. The chamber flow is normally at least 1,000 times weaker than the flow through the channels themselves, that is, about 0.1 μm/s chamber flow and 100 μm/s channel flow.

A key problem in operation of the proposed chemostat—loading of the cells into the chambers—was resolved by taking advantage of high flexibility of PDMS (**Supplementary Methods**). When the gauge pressure inside the device increases, the microchannels inflate and the 'roofs' of the capillaries bulge up, increasing capillary depth and allowing passage of cells (**Fig. 1c**). We found that the depth of the capillaries increased linearly with the gauge pressure, reaching ~2.5 μm at 8 p.s.i. (**Supplementary Fig. 3** online). When the gauge pressure is dropped to zero, the channels deflate, and the capillaries become inaccessible to cells again. (Compliance of PDMS under pressure was used previously for construction of membrane valves in two-layer devices[19].)

Device characterization

As a test we loaded into the chambers 1.5-μm monodisperse polystyrene beads. We used bead suspensions of 10^6–10^8 particles per milliliter resulting in 0.18–14 beads per chamber on average (**Supplementary Fig. 4** online). As expected, the distributions of beads in chambers followed the Poisson law. At concentrations ≪1 bead per chamber, when most of the chambers are empty, the majority of the chambers with beads have only one bead inside. This distribution suggests a possibility of having most colonies originate from single cells. Although chambers are predominantly

empty in this case, the number of colonies can be increased by augmenting the functional area of the device and the number of chambers. We could indeed capture single cells in chambers and observed colonies developing from them in many experiments. In a representative experiment shown in **Figure 2**, a single cell introduced into a chamber divided multiple times, with its progeny initially forming a branched network of nonmotile cells that then disintegrated as the cells initiated random movement. Cell densities approaching complete (dense) chamber packing (estimated at ~2.5×10^{11} cells/ml for *E. coli*) were also consistently achieved with several other bacterial and yeast strains (**Supplementary Fig. 2**).

Next we expressed in *E. coli* a truncated *V. fischeri lux* operon that is involved in quorum sensing[20–22] to study the response of a growing colony to a quickly diffusing substance and to track the rate of colony growth. In quorum sensing, bacteria at high densities exchange a membrane-permeable compound termed autoinducer and this leads to overexpression of genes in the *lux* operon, including *luxR*, the gene encoding the autoinducer receptor LuxR. We took advantage of this inducible upregulation by fusing *luxR* to a gene encoding a low-stability GFP(LVA) mutant[23]. We estimated the steady state (**Supplementary Fig. 5** online) and dynamic (**Fig. 3a**) responses to exogenously added *V. fischeri*–specific autoinducer, *N*-3-oxo-hexanoyl homoserine lactone. In a dynamic response experiment, when regular medium was replaced with medium containing 10 nM of autoinducer, after a latency period of ~20 min there was a fast exponential increase in fluorescence over approximately 3–4 orders of magnitude (fitted with $\exp(28.7\ \mathrm{h}^{-1} \times t)$) followed by slower exponential growth ($\exp(0.8\ \mathrm{h}^{-1} \times t)$; **Fig. 3a**). Concentration of autoinducer (10 nM) was below saturation value, but caused uniform response across the cell population (**Supplementary Fig. 5**). The initial increase in fluorescence was likely due to transcriptional *luxR* and *gfp* upregulation (compare to ~1,000-fold transcriptional upregulation of the *lux* operon reported in ref. 23). The later, slower exponential rise was probably due to cell proliferation (**Fig. 3b,c**). After autoinducer removal, a transient biphasic behavior for
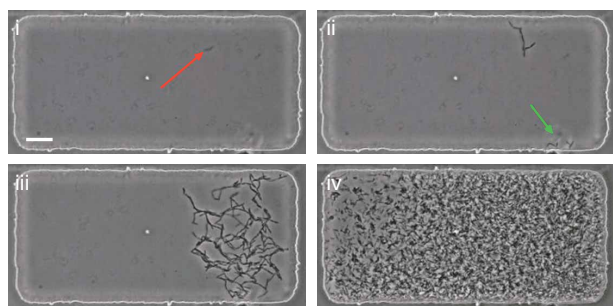
Figure 2 | A representative experiment showing development of a JM109 *E. coli* colony inside a chamber at 35 °C from a single cell captured at the beginning of the experiment. Bar, 20 μm. The time frames are taken in sequence shown: 0 h (i), 3 h (ii), 5 h (iii) and 8 h (iv). The originating cell (red arrow) grows into a cell cluster that breaks into two (one indicated by a green arrow) and then forms a complex cell network that ultimately grows to fill the entire chamber.

approximately 45 min was followed by a rapid decay of fluorescence characterized by two exponential rates. The slower rate (-1.07 ± 0.2 h^{-1}) observed first was equal to that reported for the degradation rate of the GFP(LVA) (0.018 min^{-1} reported in ref. 23). The subsequent faster rate may be due to a yet unknown mechanism of GFP(LVA) degradation. The chemostat design thus allows analysis of the dynamic responses of growing colonies to exogenous signals and recording of the growth curves of the colonies over extended periods of time.

Testing chemostatic conditions

The exponential increase of GFP(LVA) fluorescence in growing colonies at constant autoinducer concentration (**Fig. 3a**) suggests uniform rates of cell proliferation throughout the chambers. In an extreme nonuniform case of proliferation at a colony periphery only, fluorescence intensity would increase linearly. To further assess proliferation uniformity, accessibility of nutrients and autoinducer to the cells, and experimental variability, we recorded

colony growth curves at a constant autoinducer concentration (10 nM) in chambers of three different widths ($w = 70$, 105 and 140 μm) and at two different temperatures (20 and 35 °C), using three different chips at each temperature (**Fig. 3b,c** and **Supplementary Fig. 6** online). The growth was exponential over at least two orders of magnitude in all cases. The growth rates were close to those observed in exponential batch culture: 0.72 ± 0.07 h^{-1} versus 0.8 h^{-1} at 20 °C and 1.19 ± 0.02 h^{-1} versus 1.3 h^{-1} at 35 °C, on the chip and in the batch culture, respectively. Deviations from the exponential growth became pronounced at very high cell concentrations, typically only three- to tenfold (depending on temperature and chambers size) below the plateau corresponding to a dense packing of the cells in the chambers (**Fig. 2**). There was exponential growth over a range of 3–4 orders of magnitude of cell concentration in colonies starting with 1–3 cells (**Supplementary Fig. 7** online). Fluorescence in the plateau regions was highly uniform throughout the chambers, suggesting uniform autoinducer access even at highest cell densities.

Variability in growth rates (and, ultimately, colony sizes) between different equally sized chambers on the same chip and on different chips was similar: 5–10% at 20 °C and 25–30% at 35 °C (**Supplementary Fig. 6**). At 20 °C, the growth curves were also highly consistent for chambers of all three widths (**Fig. 3b**). The exchange of chemicals between the chambers and channels occurs through capillaries by diffusion and its efficiency decreases with width. Therefore, compromised medium conditions anywhere in the 70- and 105-μm chambers would imply even less favorable cell environments in substantial portions of the 140-μm chambers, resulting in slower colony growth for the 140-μm chambers. Hence the overlapping growth curves are a strong indication for the existence of essentially chemostatic conditions throughout the 70- and 105-μm wide chambers at 20 °C at all cell densities (**Fig. 3b**). The shape of the growth curve for the 70-μm chambers at 35 °C (**Fig. 3c**) is the same as at 20 °C (up to rescaling of the growth rates; **Fig. 3b**), suggesting that the conditions remain largely chemostatic in these chambers as well. As the chamber width increases, the colony growth rates at 35 °C systematically decrease,
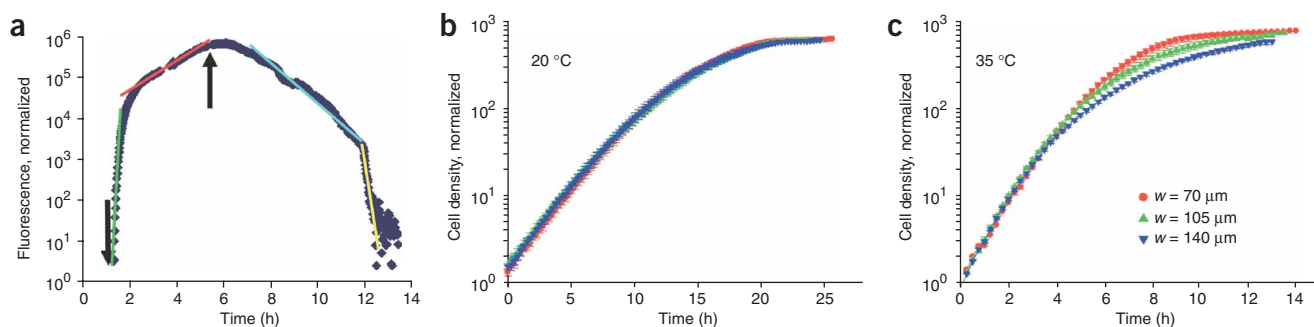
Figure 3 | Response of cells to addition and removal of exogenous signal, and growth curves of colonies under different conditions. (**a**) A representative time dependence of the whole-colony fluorescence intensity (in a $100 \times 200 \times 6$ μm chamber) owing to autoinducer-dependent GFP(LVA) expression in response to addition (down arrow) and removal (up arrow) of 10 nM homoserine lactone to the medium fed to the channels. The straight lines indicate exponential curves fitted to the data set. The quantitative parameters determined from fitting are given in the text. (**b,c**) Study of the random and systematic variations in colony growth in chambers of different sizes at 20 °C and 35 °C. The chambers had dimensions $w \times 100 \times 5$ μm. To plot the curves, recorded fluorescence intensities were normalized to represent cell density by division by chamber volume to compare chambers of different size. The cell density of approximately 1 was taken to be the lowest initial cell density. To account for different initial numbers of cells in the chambers and thus compare proliferation rates at the same cell density, the curves were shifted along the time axis to the point at which their early time segments overlapped. The initial number of cells in the chambers varied from 15 to 30. The averaging was done over 12 chambers on three chips for all sizes at 20 °C, and over 7, 6 and 6 chambers on three chips for $w = 70$, 105 and 140 μm, respectively, at 35 °C. Error bars are s.e.m.

as colony size approaches the capacity of the chamber (**Fig. 3c**). This result suggests that owing to high intrinsic rates of metabolism and, possibly, reduced diffusion rates in dense colonies growing at 35 °C, chemostasis may be somewhat perturbed in chambers with $w > 70$ μm. Nevertheless, chemostasis is quite robust in narrow chambers, at 20 °C and at lower cell densities.

DISCUSSION

Functionality of the proposed chemostat is somewhat similar to that of a previously described device[16], assembled from two PDMS parts with a sandwiched porous membrane and a cover glass. Nevertheless, the chemostat we propose has a few important advantages. The entire functional area (**Fig. 1a–c**) is made of a single cast of PDMS sealed with a cover glass (no assembly required) and can be readily integrated with other microfluidic elements. The chemostat permits growth of high-density bacterial and yeast colonies with large numbers of cells in chambers matching the field of view and working distance of standard high-resolution objective lenses. Also, loading cells into the chambers is simple and reliable.

The architecture of the microchemostat described here resembles complex structures of bacterial and yeast biofilms, where cells often grow in clumps separated by 'channels' supplying nutrients and removing waste. The dimensions of the chambers are similar to the size of the microcolonies found in some biofilms. This device therefore allows analysis of development of bacterial and yeast species in an environment resembling that of naturally occurring high-density colonies. Additionally, the single-cell resolution achieved on the chip can allow analysis of the effects of noise in gene expression[24–26], the onset of aging[27], appearance of spontaneous mutations or the segregation of a population into particular subpopulations (for example, sporulation[28]). The flexible design allows control of multiple parameters regulating colony growth and development, including the chamber size (and thus the maximum size of the colonies), and temperature. Development of devices with a similar design should allow the study of other nonadherent cell types, including mammalian cells, such as cells of hematopoietic origin.

METHODS

Device fabrication. The microchannel device was made of two layers of PDMS (Dow Corning Sylgard 184) using soft lithography[29] and sealed to a #1.5 microscope cover glass (**Fig. 1**). The master mold for the first layer (for cells and medium) was a silicon wafer with a two-level relief with heights of 0.65 and 6 μm (**Supplementary Fig. 1**). The mold was spin-coated with ~150 μm–thick layer of PDMS prepolymer, which was then cured at 80 °C. The master mold for the second, water circulation layer had 300 μm–thick relief. It was used to make a ~5 mm–thick PDMS cast that was cut into individual chips. The chips were aligned and placed on top of the 150 μm–thick PDMS layer on the first wafer, which was precoated by ~15 μm–thick layer of partially cured PDMS for bonding. After curing, monolith two-layer PDMS chips were formed[19]. (See **Supplementary Methods** for more details). After use the PDMS chips were separated from the glass, washed in a mild detergent and reused.

Flow driving. Working liquids (the media and cell suspensions) were kept in 30-ml plastic syringes connected to the microfluidic devices by tygon tubing with an inner diameter of 0.5 mm. The flow was driven by pressure differences between the inlets and outlets. The syringes were held upright attached to platforms sliding on vertical rails to generate the hydrostatic pressure[30]. The syringes could be either opened to the atmosphere or filled with compressed air with pressure in a range from 0 to 12 p.s.i.

Microscopy and image analysis. Fluorescence, bright-field and phase-contrast micrographs were captured at 20×, 40× and 60× magnification with a Nikon Eclipse TE2000 epifluorescence microscope equipped with electronic shutters and a Spot RT camera (Diagnostic Instruments). The rate of colony growth was studied by taking series of fluorescence images of the same chamber at fixed time intervals (usually about 3 min) and with a constant exposure. We assumed that the number of cells is proportional to the total fluorescence of the area. The latter was calculated by summing the intensity values for all the pixels in the image of the chamber and subtracting the background level.

Additional methods. Descriptions of bacterial and yeast species used and the construction of the plasmid are available in **Supplementary Methods**.

Note: Supplementary information is available on the Nature Methods website.

1. Stoodley, P., Sauer, K., Davies, D.G. & Costerton, J.W. Biofilms as complex differentiated communities. *Annu. Rev. Microbiol.* **56**, 187–209 (2002).
2. Reynolds, T.B. & Fink, G.R. Bakers' yeast, a model for fungal biofilm formation. *Science* **291**, 878–881 (2001).
3. Douglas, L.J. Candida biofilms and their role in infection. *Trends Microbiol.* **11**, 30–36 (2003).
4. Anderson, G.G. *et al.* Intracellular bacterial biofilm-like pods in urinary tract infections. *Science* **301**, 105–107 (2003).
5. Jelsbak, L. & Sogaard-Andersen, L. Pattern formation: fruiting body morphogenesis in *Myxococcus xanthus*. *Curr. Opin. Microbiol.* **3**, 637–642 (2000).
6. Udvardi, M.K. & Day, D.A. Metabolite transport across symbiotic membranes of legume nodules. *Annu. Rev. Plant Physiol. Plant Mol. Biol.* **48**, 493–523 (1997).
7. Tebo, B.M., Linthicum, D.S. & Nealson, K.H. Luminous bacteria and light emitting fish: ultrastructure of the symbiosis. *Biosystems* **11**, 269–280 (1979).
8. Scherz, R., Shinder, V. & Engelberg, D. Anatomical analysis of *Saccharomyces cerevisiae* stalk-like structures reveals spatial organization and cell specialization. *J. Bacteriol.* **183**, 5402–5413 (2001).
9. Hastings, J.W. & Nealson, K.H. Bacterial bioluminescence. *Annu. Rev. Microbiol.* **31**, 549–595 (1977).
10. Sternberg, C. *et al.* Distribution of bacterial growth activity in flow-chamber biofilms. *Appl. Environ. Microbiol.* **65**, 4108–4117 (1999).
11. Millar, M.R., Linton, C.J. & Sherriff, A. Use of a continuous culture system linked to a modified Robbins device or flow cell to study attachment of bacteria to surfaces. *Methods Enzymol.* **337**, 43–62 (2001).
12. Li, N., Tourovskaia, A. & Folch, A. Biology on a chip: microfabrication for studying the behavior of cultured cells. *Critical Reviews in Biomedical Engineering* **31**, 423–488 (2003).
13. Andersson, H. & van den Berg, A. Microfluidic devices for cellomics: a review. *Sens. Actuators B Chem.* **92**, 315–325 (2003).
14. Sia, S.K. & Whitesides, G.M. Microfluidic devices fabricated in poly(dimethyl-siloxane) for biological studies. *Electrophoresis* **24**, 3563–3576 (2003).
15. Mao, H.B., Cremer, P.S. & Manson, M.D. A sensitive, versatile microfluidic assay for bacterial chemotaxis. *Proc. Natl. Acad. Sci. USA* **100**, 5449–5454 (2003).

16. Balaban, N.Q., Merrin, J., Chait, R., Kowalik, L. & Leibler, S. Bacterial persistence as a phenotypic switch. *Science* **305**, 1622–1625 (2004).
17. Park, S. *et al.* Influence of topology on bacterial social interaction. *Proc. Natl. Acad. Sci. USA* **100**, 13910–13915 (2003).
18. Mao, H.B., Yang, T.L. & Cremer, P.S. A microfluidic device with a linear temperature gradient for parallel and combinatorial measurements. *JACS* **124** (2002).
19. Unger, M.A., Chou, H.P., Thorsen, T., Scherer, A. & Quake, S.R. Monolithic microfabricated valves and pumps by multilayer soft lithography. *Science* **288**, 113–116 (2000).
20. Miller, M.B. & Bassler, B.L. Quorum sensing in bacteria. *Annu. Rev. Microbiol.* **55**, 165–199 (2001).
21. Fuqua, C., Parsek, M.R. & Greenberg, E.P. Regulation of gene expression by cell-to-cell communication: acyl-homoserine lactone quorum sensing. *Annu. Rev. Genet.* **35**, 439–468 (2001).
22. Withers, H., Swift, S. & Williams, P. Quorum sensing as an integral component of gene regulatory networks in gram-negative bacteria. *Curr. Opin. Microbiol.* **4**, 186–193 (2001).
23. Andersen, J.B. *et al. gfp*-based *N*-acyl homoserine-lactone sensor systems for detection of bacterial communication. *Appl. Environ. Microbiol.* **67**, 575–585 (2001).
24. Elowitz, M.B., Levine, A.J., Siggia, E.D. & Swain, P.S. Stochastic gene expression in a single cell. *Science* **297**, 1183–1186 (2002).
25. Ozbudak, E.M., Thattai, M., Kurtser, I., Grossman, A.D. & van Oudenaarden, A. Regulation of noise in the expression of a single gene. *Nat. Genet.* **31**, 69–73 (2002).
26. Blake, W.J., Kaern, M., Cantor, C.R. & Collins, J.J. Noise in eukaryotic gene expression. *Nature* **422**, 633–637 (2003).
27. McMurray, M.A. & Gottschling, D.E. An age-induced switch to a hyper-recombinational state. *Science* **301**, 1908–1911 (2003).
28. Flardh, K. Growth polarity and cell division in *Streptomyces*. *Curr. Opin. Microbiol.* **6**, 564–571 (2003).
29. Xia, Y.N. & Whitesides, G.M. Soft lithography. *Angew. Chem. Int. Ed.* **37**, 551–575 (1998).
30. Groisman, A., Enzelberger, M. & Quake, S.R. Microfluidic memory and control devices. *Science* **300**, 955–958 (2003).